Design and Evaluation of a Wearable Fingertip Device for Three-Dimensional Skin-Slip Display

Yiting Mo ⬦, Aiguo Song ⬦, *Senior Member, IEEE*, Lifeng Zhu ⬦, *Member, IEEE*, Qinjie Ji ⬦, Ting Wang ⬦, and Huanhuan Qin ⬦

Abstract—Skin-slip provides crucial cues about the interaction state and surface properties. Currently, most skin-slip devices focus on two-dimensional tactile slip display and have limitations when displaying surface properties like bumps and contours. In this article, a wearable fingertip device with a simple, effective, and low-cost design for three-dimensional skin-slip display is proposed. Continuous multi-directional skin-slip and normal indentation are combined to convey the sensation of three-dimensional geometric properties in virtual reality during active finger exploration. The device has a tactile belt, a five-bar mechanism, and four motors. Co-operating with the angle-mapping strategy, two micro DC motors are used to transmit continuous multi-directional skin-slip. Two servo motors are used to drive the five-bar mechanism to provide normal indentation. The characteristics of the device were obtained through the bench tests. Three experiments were designed and sequentially conducted to evaluate the performance of the device in three-dimensional surface exploration. The experimental results suggested that this device could effectively transmit continuous multi-directional skin-slip sensations, convey different bumps, and display surface contours.

Index Terms—Wearable fingertip device, three-dimensional skin-slip, haptic display, virtual reality.

I. INTRODUCTION

HAPTIC stimuli play an important role in virtual environment interaction. In addition to visual feedback, with the help of haptic stimuli, users can perceive the object's features (such as mass, stiffness, and surface texture), which greatly improves the immersion and presence of the interaction [1].

Haptic stimuli can be mainly divided into kinesthetic stimuli and cutaneous stimuli. Compared with kinesthetic stimuli, cutaneous stimuli have been widely used in precision manipulation and surface exploration [2]. During active finger exploration, the mechanoreceptors in the finger pulp are activated so that the specific surface properties can be perceived [3]. Over the past few decades, various wearable fingertip devices with cutaneous feedback have been developed. Vibrotactile actuators are commonly used in fingertip haptic devices to display the material texture [4]. However, the sustained stimuli produced by vibration bring fatigue and discomfort quickly [5]. Compared with the vibrotactile devices, cutaneous deformation devices show a more effective way to convey perceptual cues due to the highly effective analog resolution of the skin [6]. Skin-slip can be defined as the way haptic stimuli are transmitted along the tangential direction of the skin, and it plays an important role in surface exploration and perception [7]. Based on the tactors, skin-slip devices can be mainly classified into ball-type, wheel-type, and belt-type devices. Two-degrees-of-freedom (DoF) slip devices with ball-type tactors placed under the fingertip were proposed in [8], [9]. The psychophysical experiment in [8] indicates that a slip angle up to 20° cannot be identified correctly by the subjects. The angle discrimination experiment in [9] finds the relative slip angle threshold exceeds more than 50° during active finger exploration. Haptic Revolver is a hand-held device that adopts a 1-DoF interchangeable wheel-type tactor with multiple haptic features for virtual surface exploration [10].

In addition to the ball-type and wheel-type tactors, the belt-type tactors provide an efficient way to convey skin-slip sensations due to their softness and deformability. Salazar et al. conducted the evaluation experiment of hRing to show its capability to display the illusion of virtual bumps and holes [11]. But hRing can only generate skin-slip over a short distance. Atapattu et al. introduced a wearable haptic device for surface texture recognition and edge detection [12]. ShearTouch is a 1-DoF wearable fingertip device that displays continuous skin-slip sensation via timing belt loop [13]. Slip-Pad was designed as a haptic display with four orthogonal polyester belts to convey the sensation of lateral and rotational slip on the fingertip [14]. Zhang et al. designed a wearable fingertip device with plain-woven belts to render both normal force and continuous omnidirectional motions [15]. Most skin-slip devices do not have the contact/noncontact capability which benefits the simulation of natural interaction. In addition, these devices mainly focus on two-dimensional tactile slip display.
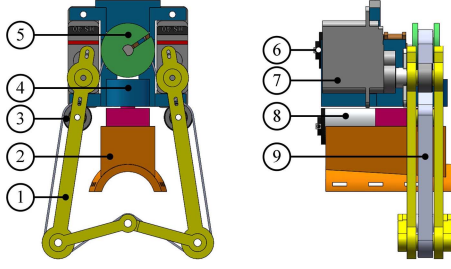
Fig. 1. General assembly of proposed device. (1) Linkage of five-bar mechanism, (2) Finger cover, (3) Bearing, (4) Motor base, (5) Belt reel, (6) DC motor #1, (7) Servo motor, (8) DC motor #2, (9) Belt.
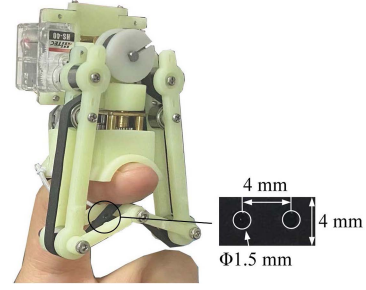

Fig. 2. Prototype of wearable fingertip device.

The typical fingertip devices with the contact/noncontact capability have moving tactors. Chinello et al. designed a wearable tactile device for virtual exploration and conducted the curvature discrimination experiment [16]. Solazzi et al. introduced Active Thimble, a portable interface to display the contact/noncontact transition and the local orientation of a virtual surface [17]. Based on Active Thimble, Haptic Thimble improves the driving solution to render edges and textures [18]. Tanaka et al. proposed a wearable haptic device to perceive small and wide surface undulations [19]. Gaffary et al. proposed HapTip, a 2-DoF wearable haptic fingertip device, to convey the tactile alphabets [20]. The devices discussed above can naturally and realistically convey the geometric properties of three-dimensional surfaces, however, large-scale three-dimensional surface exploration remains a challenge due to the limited workspace of the tactors.

Cutaneous cues can highly affect the perception of surface properties, such as bumps and contours. Currently, most skin-slip devices focus on two-dimensional tactile slip display and have limitations in presenting the surface properties like bumps and contours [15]. The cutaneous fingertip devices with moving tactors are capable of three-dimensional surface exploration but have limitations when interacting with large-scale three-dimensional surfaces due to the limited workspace of the tactors. We propose a wearable fingertip device with a simple, effective, and low-cost design for three-dimensional skin-slip display in this article. This device adopts a configuration that combines multi-directional continuous skin-slip and normal indentation by using a belt loop and a five-bar mechanism. Due to the finger interference, an angle mapping strategy is applied to render continuous multi-directional skin-slip. With this device, the user can freely interact with three-dimensional virtual surfaces and perceive their surface properties like bumps and contours.

II. DEVICE IMPLEMENTATION

A. Mechanical Design

The mechanical assembly of the proposed device is shown in Fig. 1. The device mainly includes a five-bar mechanism, a finger cover, a motor base, a rubber belt, a belt reel, two direct current (DC) motors, two servo motors, and six bearings. The servo motors (HS-40, Hitec) are fixed on the motor base and used to drive the five-bar mechanism to provide normal indentation on the fingertip. The DC motor #1 (GA12-N20 with gearbox, ASLONG) is also fixed on the motor base to drive the rubber belt

at the given velocity. For better motion transmission, a silicon ring is placed in the groove of the belt reel. The DC motor #2 (GA12-N20 with worm gearbox, ASLONG) is inserted into the finger cover, and its shaft is connected to the motor base. When the DC motor #2 is activated, the belt can be rotated to the given angle around the normal direction of the finger. To establish a tight fit, the finger cover has elastic band mounting holes. The bearings (MR84ZZ, UKG) are placed at the corners of the five-bar mechanism for smooth skin-slip. The belt has 4 mm width and 0.5 mm thickness. To improve the perception of slip distance and velocity, equidistant points are marked on the belt [14].

Most parts of the device are 3D-printed using the resin material. The displacement and orientation of the belt are closed-loop controlled by PID controllers. The device prototype (shown in Fig. 2) is 58.2 g in weight and $70.6 \times 32.9 \times 39.1$ mm in dimensions.

Fig. 3. Kinematics of proposed device.

B. Kinematics

1) Forward Kinematics: The linkage length and angle/coordinate assignment of the five-bar mechanism are shown in Fig. 3. Let D be the origin of cartesian coordinate system and (X_A, Y_A) be the coordinates of A. The following equations can be derived:

$$\begin{cases} l_2 \cos\theta_1 + l_3 \cos\theta_3 + l_4 \cos\theta_4 = l_1 + l_5 \cos\theta_2 \\ l_2 \sin\theta_1 - l_3 \sin\theta_3 + l_4 \sin\theta_4 = l_5 \sin\theta_2 \end{cases} \quad (1)$$

The combination of the above equations gives:

$$a \cos\theta_3 + b \sin\theta_3 + c = 0 \quad (2)$$

where

$$\begin{cases} a = 2\left(l_2 \cos\theta_1 - l_1 - l_5 \cos\theta_2\right) l_3 \\ b = 2\left(l_5 \sin\theta_2 - l_2 \sin\theta_1\right) l_3 \\ c = \left(l_2 \cos\theta_1 - l_1 - l_5 \cos\theta_2\right)^2 \\ \quad + \left(l_2 \sin\theta_1 - l_5 \sin\theta_2\right)^2 + l_3^2 - l_4^2 \end{cases} \quad (3)$$

Then, θ_3 can be expressed as:

$$\theta_3 = 2\arctan\left(\frac{-b + \sqrt{a^2 + b^2 - c^2}}{c - a}\right) \quad (4)$$

Therefore, according to the input angles of the five-bar mechanism (θ_1 and θ_2), the coordinate of A (Y_A) can be finally calculated to be:

$$Y_A = l_2 \sin\theta_1 - l_3 \sin\theta_3$$
$$= l_2 \sin\theta_1 - l_3 \sin\left[2\arctan\left(\frac{-b + \sqrt{a^2 + b^2 - c^2}}{c - a}\right)\right] \quad (5)$$

2) Inverse Kinematics: X_A and Y_A can be written to be:

$$\begin{cases} X_A = l_2 \cos\theta_1 + l_3 \cos\theta_3 \\ Y_A = l_2 \sin\theta_1 - l_3 \sin\theta_3 \end{cases} \quad (6)$$

The combination of the above equations gives:

$$\left(X_A - l_2 \cos\theta_1\right)^2 + \left(Y_A - l_2 \sin\theta_1\right)^2 = l_3^2 \quad (7)$$

Then, θ_1 can be expressed to be:

$$\theta_1 = 2\arctan\frac{b_1 + \sqrt{b_1^2 - 4a_1 c_1}}{2a_1} \quad (8)$$

where

$$\begin{cases} a_1 = X_A^2 + Y_A^2 + l_2^2 - l_3^2 + 2l_2 X_A \\ b_1 = 4l_2 Y_A \\ c_1 = X_A^2 + Y_A^2 + l_2^2 - l_3^2 - 2l_2 X_A \end{cases} \quad (9)$$

Similarly, θ_2 can be expressed to be:

$$\theta_2 = 2\arctan\frac{b_2 - \sqrt{b_2^2 - 4a_2 c_2}}{2a_2} \quad (10)$$

where

$$\begin{cases} a_2 = (X_A - l_1)^2 + 2l_5(X_A - l_1) + Y_A^2 + l_5^2 - l_4^2 \\ b_2 = 4l_5 Y_A \\ c_2 = (X_A - l_1)^2 - 2l_5(X_A - l_1) + Y_A^2 + l_5^2 - l_4^2 \end{cases} \quad (11)$$

C. Angle Mapping Strategy

Due to the finger interference, the tactile belt cannot rotate $360°$ around the normal direction of the finger. According to the research in [14] and [8], the user cannot discriminate an angled slip over the fingertip from a straight stimulus up to approximately $50°$ during active finger exploration. Therefore, an angle mapping strategy was designed and applied to realize multi-directional motions. This strategy extended the original angle range evenly to the range of $-90° - 90°$, which could be expressed as: $\theta_m = k\theta_o$. θ_o was the original angle, θ_m was the mapped angle, and k was set to be 9/4.

Fig. 4. Soft sensing module based on pressure sensor.

Fig. 5. Calibration setup of soft sensing module.

D. Device Characteristics

To specifically test the characteristics of the proposed device, a soft sensing module was fabricated (as shown in Fig. 4). The soft sensing module was mainly composed of a flexible finger-shaped part, an air chamber, a syringe, and hoses. The flexible finger-shaped part was designed to withstand external loads. A pressure sensor (BME280, Bosch) was placed within the air chamber to measure the force and displacement applied to the module. To reduce the influence of the air chamber deformation on the force/displacement measurement, the air chamber was covered with a rigid resin box. The syringe was used to adjust the initial pressure of the module. The finger-shaped part, air chamber, and syringe were connected via hoses with inner and outer diameters of 2 mm and 4 mm, respectively. When an external load was applied on the module, the finger-shaped part was compressed. Assuming that the mass of the air within the module was constant, the volume change of the air in the finger-shaped part would lead to the change of the pressure in the air chamber, which was further measured by the pressure sensor.

The soft sensing module was calibrated on a force-displacement test bench (as shown in Fig. 5). A force gauge (ZTS-50 N, IMADA Inc.) and a digital caliper were fixed on the test bench. The force/displacement could be slowly applied to the module by rotating the bench wheel. During calibration, the initial pressure was set to 1111.65 hPa. Two rounds of calibration were conducted to obtain the force-pressure relationship and displacement-pressure relationship. Each round of calibration was repeated three times, and the average value was calculated
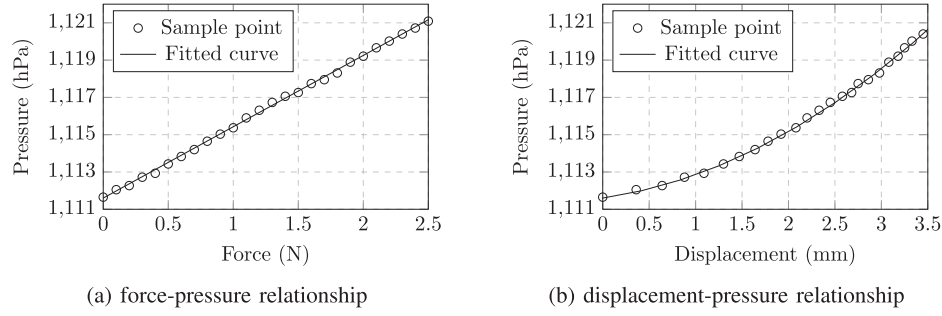
(a) force-pressure relationship

(b) displacement-pressure relationship

Fig. 6. Calibration results of soft sensing module.

(a) step response of belt displacement

(b) step response of belt orientation
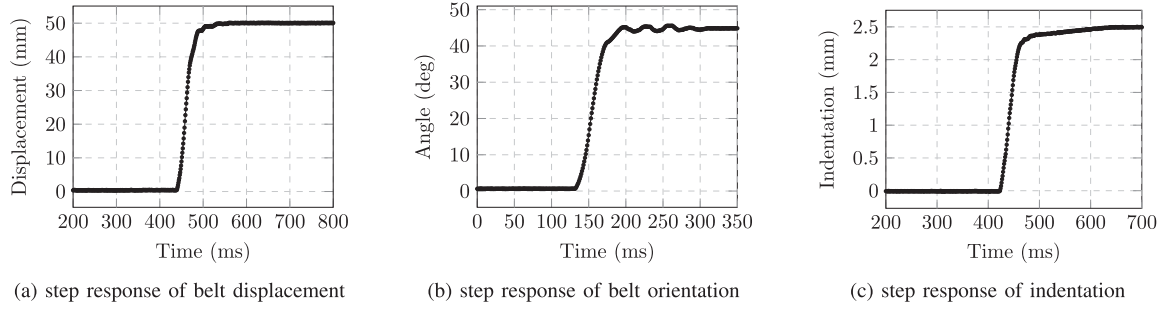
(c) step response of indentation

Fig. 7. Step response performance of proposed device.

as the final result. The calibration results were displayed in Fig. 6. The force-pressure relationship and displacement-pressure relationship could be expressed as:

$$P = 3.8255F + 1111.6, \ R^2 = 0.9991 \tag{12}$$

$$P = 0.5314D^2 + 0.7178D + 1111.6, \ R^2 = 0.9991 \tag{13}$$

where P, F, and D were pressure, force, and displacement, respectively. R^2 was the coefficient of determination, which quantified a goodness of fit.

The finger-shaped part of the soft sensing module was placed under the finger cover to evaluate the actual performance of the device. The device was controlled to make contact with the finger-shaped part without applying force. The minimum input was applied to the servo motor, and the input was increased until a clear pressure difference was observed. The observed pressure difference was about 0.17 hPa, corresponding to an indentation resolution of about 0.2 mm. Under the maximum input of the servo motor, the pressure difference was observed to be 5.61 hPa, corresponding to 1.5 N indentation force and 2.68 mm indentation range. Furthermore, magnetic encoders (AS5047P, AMS) were used to measure the performance of the belt displacement and belt orientation. Small magnets were attached to the belt reel and the linkage of five-bar mechanism (indentation point). The step response of the belt displacement, belt orientation, and indentation was shown in Fig. 7. The rise time (10%–90%) of the belt displacement, belt orientation, and indentation was 36 ms, 32 ms, and 35 ms, respectively. Hence, the control bandwidth was set to be 10 Hz. Due to the motor backlash, there was a belt displacement error and a belt orientation error, especially in

reverse rotation. The observed belt displacement error and belt orientation error were no larger than 2 mm and 3°, respectively.

The technical specifications of the prototype are summarized in Table I.

TABLE I
TECHNICAL SPECIFICATIONS OF THE PROTOTYPE

Item	Value
Size	70.6 × 32.9 × 39.1 mm
Weight	58.2 g
Indentation resolution	0.2 mm
Indentation range	2.68 mm
Indentation force	1.5 N
Belt displacement resolution	0.1 mm
Belt displacement accuracy	± 2 mm
Belt orientation resolution	0.25°
Belt orientation accuracy	± 3°
Control bandwidth	10 Hz

III. EVALUATION EXPERIMENTS

Three experiments were designed and sequentially conducted to evaluate the performance of the proposed device in three-dimensional virtual surface exploration. 10 subjects (8 males and 2 females, average age of 25, all right-handed) participated in the experiments. None of them reported any perceptual deficiencies. During the experiments, all subjects were asked to wear noise-canceling headphones. Pink noise was played to avoid auditory cues produced by the device. A desktop haptic device (Touch X, 3D system Inc.) was used as the tracking system to ensure a stable interaction status. The scale of the virtual environment matched the workspace of Touch X so that the subjects could

Fig. 8. Setup of two-dimensional surface exploration.

TABLE II
STATISTICS OF WILCOXON SIGNED-RANK TEST

path	median		z	p value
	1-DoF skin-slip[1]	2-DoF skin-slip[2]		
horizontal	6.0	6.5	0.491	0.623
vertical	2.0	5.0	2.842	0.004
sharp-edged	4.0	6.0	2.701	0.007
curved	3.0	6.0	2.739	0.006

[1] 1-DoF skin-slip generates tactile slip perpendicular to the finger.
[2] 2-DoF skin-slip generates multi-directional tactile slip over the finger pulp.

TABLE III
STATISTICS OF FRIEDMAN TEST AND POST HOC TEST WITH BONFERRONI CORRECTION

Friedman test			Bonferroni post hoc test	
condition	$\mathcal{X}^2$	p value	path	p value
1-DoF skin-slip	27.415	<0.001	vertical vs. curved	0.599
			vertical vs. sharp-edged	0.034
			vertical vs. horizontal	<0.001
			curved vs. sharp-edged	1.000
			curved vs. horizontal	0.006
			sharp-edged vs. horizontal	0.182
2-DoF skin-slip	17.892	<0.001	vertical vs. curved	0.414
			vertical vs. sharp-edged	0.116
			vertical vs. horizontal	0.001
			curved vs. sharp-edged	1.000
			curved vs. horizontal	0.278
			sharp-edged vs. horizontal	0.846

easily reach the target areas in the experiments. The subject's left index finger was attached to the end-effector of Touch X with velcro tapes. Each subject was asked to keep his/her index finger in a horizontal posture without changing its orientation. In the experiments, the belt was not initially in contact with the fingerpad. Only when the finger proxy was in contact with the virtual surface would the belt come into contact with the fingerpad. The skin-slip would be provided when a relative displacement occurred between the proxy and the surface.

A. Two-Dimensional Surface Exploration

This experiment attempted to verify the effectiveness of the device in interacting with two-dimensional surfaces without bumps.

1) Experimental Setup and Methods: As shown in Fig. 8, the subject was free to click the score buttons on the interface after tracing the paths. Four paths with horizontal, vertical, sharp-edged, and curved characteristics were selected for the task. Each path was scaled to fit within a 3×3 cm square. The button represented the answer to the question: how consistent is the skin-slip with the visual stimulus? Score 1 meant "not consistent at all" and score 7 meant "highly consistent". The visual stimulus was provided to guide the subject's finger movement. The normal indentation during the interaction was set to be 1 mm.

The task was to trace each path and choose the appropriate score for the question. The subject was encouraged to carefully perceive the consistency between the skin-slip sensation and the finger motion on the specific path, and give the score based on the visual-tactile consistency level. Since both 1-DoF and 2-DoF skin-slip could effectively convey directional slipping stimuli during 2-DoF finger active exploration [9], [10], two rounds of tasks were provided. In 1-DoF skin-slip, the belt velocity was set to be the horizontal component of the finger velocity, and the belt angle was limited to the direction perpendicular to the finger. In 2-DoF skin-slip, the belt was rotated in the opposite direction of the finger movement, and the belt angle was calculated based on the angle mapping strategy. Each subject needed to perform two rounds of tasks randomly. After all subjects completed the tasks, their scores were recorded for analysis.

2) Results and Discussion: A non-parametric Wilcoxon signed-rank test on the median value was conducted to reveal the difference between two feedback conditions. The median of each path and the results of Wilcoxon signed-rank test under each condition are shown in Table II. Generally, the scores of the four paths in 2-DoF skin-slip (median = 6.5, 5.0, 6.0, and 6.0, respectively) were relatively higher than those in 1-DoF skin-slip (median = 6.0, 2.0, 4.0, and 3.0, respectively). The scores indicated that 2-DoF skin-slip (mean = 5.875) was more consistent with the sensation of slip on a surface than 1-DoF skin-slip (mean = 3.75). In the perception of the vertical, sharp-edged, and curved paths, the visual-tactile consistency levels under 2-DoF skin-slip were statistically significantly higher than those under 1-DoF skin-slip (vertical: $z = 2.842$, $p = 0.004$; sharp-edged: $z = 2.701$, $p = 0.007$; curved: $z = 2.739$, $p = 0.006$). While no significant difference was revealed in the perception of the horizontal path ($z = 0.491$, $p = 0.623$). It could be concluded that 2-DoF skin-slip under the angle mapping strategy played a crucial role in improving the visual-tactile consistency levels compared with 1-DoF skin-slip.

A non-parametric Friedman test was performed to further determine whether there were significant differences in the visual-tactile consistency levels across the paths. As shown in Table III, the Friedman test revealed the statistical difference across the four paths under 1-DoF skin-slip ($p < 0.001$), as well as under 2-DoF skin-slip ($p < 0.001$). Then, the multiple comparison issue was corrected by Bonferroni correction. Under 1-DoF skin-slip, Bonferroni post hoc test showed statistically significant differences in vertical vs. sharp-edged ($p = 0.034$), vertical vs. horizontal ($p < 0.001$), and curved vs. horizontal ($p = 0.006$). However, under 2-DoF skin-slip, Bonferroni post hoc test identified a significant difference only in vertical vs. horizontal ($p = 0.001$). The results indicated that when rendering the vertical path, the angle mapping strategy did not perform as
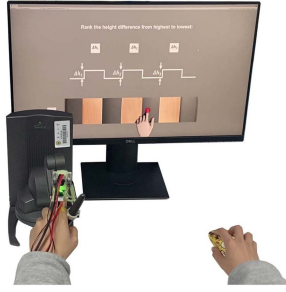
Fig. 9.   Setup of normal indentation experiment.

(a) Box plot of correct ratio
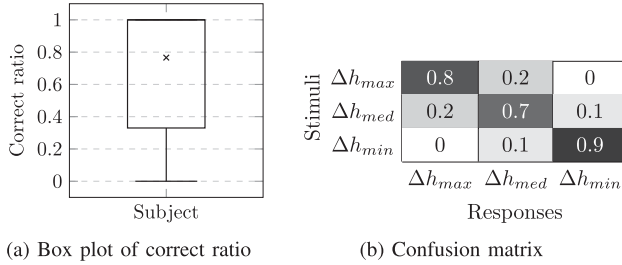
(b) Confusion matrix

Fig. 10.   Box plot and confusion matrix of normal indentation experiment.

well as rendering the horizontal, sharp-edged, and curved paths. This experiment further verified the effectiveness of the angle mapping strategy in rendering multi-directional skin-slip. The strategy was also employed in the following experiments.

B. Normal Indentation Experiment

This experiment aimed to present the performance of the device in providing normal indentation during active finger exploration.

1) Experimental Setup and Methods: As shown in Fig. 9, there was a virtual surface, a finger proxy, a red circular indicator, an illustration figure, and several buttons on the interface. The surface with regular grooved textures had a total length of 20 cm, and the parts with wood grain were lifted to different heights. To avoid unstable movement, a circular indicator was initially set on the left side of the surface. When the "start" button was clicked, the indicator moved to the right side of the surface at a constant speed of 50 mm/s. There were three buttons, named Δh_1, Δh_2, and Δh_3, on the top of the interface. These buttons corresponded to the heights of the wood grain parts.

The normal indentation was controlled by the equipped servo motors and the five-bar mechanism. They produced a maximum indentation of 1.6 mm, which specified the upper limit of indentation in this experiment. Therefore, the height of the wood grain part was set to be 1.6 mm ($\Delta h_{\max}$), 1.2 mm (Δh_{med}), and 0.8 mm ($\Delta h_{\min}$), respectively. Note that $\Delta h_{\max}$, Δh_{med}, and $\Delta h_{\min}$ were randomly assigned to the three wood grain parts. The subjects needed to slide across the grooved surface two times and then rank the height of the wood grain part from highest to lowest. The rank results were recorded for analysis.

2) Results and Discussion: The box plot of the correct ratio of all subjects is shown in Fig. 10(a). The average correct ratio and the median value were 76.6% and 100%, respectively, which
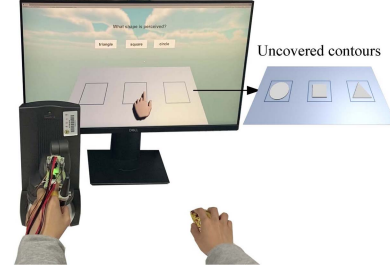

Fig. 11.   Setup of three-dimensional surface exploration.

showed a relatively high level of discrimination across different normal indentations. The device performed well to convey clear normal indentation information during active finger exploration.

The specific performance in height discrimination is shown in Fig. 10(b). "Stimuli" represented the assigned height, and "Responses" represented the discriminated height. The entries along the main diagonals were the correct ratios, while other entries were error ratios. The accuracy of $\Delta h_{\min}$ reached the highest level (90%). While the accuracy of $\Delta h_{\max}$ and Δh_{med} were 80% and 70%, respectively. But they were still much higher than the chance level and demonstrated good discrimination performance. The performance of the subjects when distinguishing $\Delta h_{\min}$ was better than $\Delta h_{\max}$ and Δh_{med}. This can be explained by the Fechner's law, which proves that a greater difference is required to perceive the same difference when the physical quantity increases [21]. Generally, the experimental results verified that the device could allow the subjects to feel an undulating surface during active finger exploration, and the subjects were able to discriminate the surface height effectively.

C. Three-Dimensional Surface Exploration

This experiment was designed to evaluate the capability of the device in displaying the geometric features of three-dimensional surfaces during active finger exploration via applying skin-slip and normal indentation.

1) Experimental Setup and Methods: As shown in Fig. 11, the geometric features of the surfaces were invisible to avoid visual distraction. Therefore, the subjects needed to explore within three square-shaped areas ($5 \text{ cm} \times 5 \text{ cm}$) and discriminate the geometric features only by cutaneous cues. The buttons at the top of the interface corresponded to the specific contours in Fig. 11. The contours were modeled as a square, a triangle, and a circle with the same height, which corresponded to the normal indentation of 1.6 mm. The table in the interface corresponded to the normal indentation of 0.4 mm.

Before the task, a pre-training period of 5 minutes was offered. The contours were visible, and the subjects were free to perceive the relation between the contours and the cutaneous cues. Then, the contours were invisible to highlight the cutaneous cues. The contours within the square-shaped areas were randomly assigned. Each subject was asked to explore within the area, trace the contour, and chose the corresponding button. The time started when the finger proxy touched the square-shaped area, and ended after the subject selected the button. The exploratory trajectories, the task time, and the button selections were recorded.
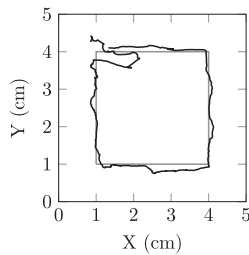
Fig. 12.   Trajectory from one subject (take square as an example). Gray line is contour and black line is exploratory trajectory.
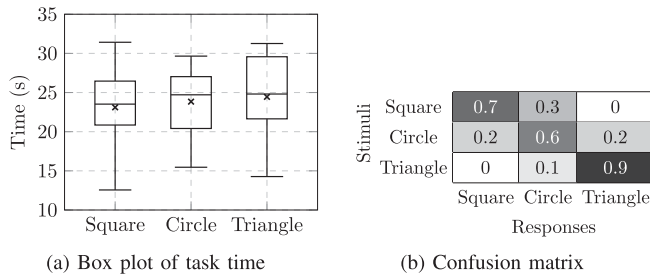

(a) Box plot of task time   (b) Confusion matrix

Fig. 13.   Box plot and confusion matrix of three-dimensional surface exploration.

2) Results and Discussion: The typical trajectory of one subject is shown in Fig. 12. Initially, this subject explored horizontally to find the contour based on the level of bump sensation. Then, he performed exploratory movements in various directions and adjusted his movements based on the sensations conveyed via the three-dimentional skin-slip display.

The box plot of the task time for each contour is presented in Fig. 13(a). The box plot reported no outliers. The average time to identify the square, circle, and triangle was 23.51 s, 23.84 s, and 24.45 s, respectively. All data passed the Shapiro-Wilk normality test and Mauchly's test of Sphericity ($p = 0.218$). The one-way repeated-measures ANOVA revealed no statistically significant difference across the time for each contour ($p = 0.814$), which indicated that the subjects did not have a reduced exploration efficiency on a specific contour.

The confusion matrix for the contours is shown in Fig. 13(b). The overall average correct ratio for the contours was 73.3% (70% for the square, 60% for the circle, and 90% for the triangle). The only incorrect response simulated by the triangle contour was "Circle". The sharp corners of triangle made it the most recognizable. The subjects were more likely to be confused between the "Square" contour and the "Circle" contour due to the morphological similarity between these two contours.

IV. CONCLUSION

A wearable fingertip device for three-dimensional skin-slip display is proposed in this article. The continuous multi-directional skin-slip and normal indentation are combined to convey the sensation of three-dimensional surface properties in VR during active fingertip exploration. The device adopts a structure that places the actuators on the back of the finger. One DC micro motor is equipped to drive the belt at the given velocity and the other is equipped to rotate the belt to the given angle around the normal direction of the finger. Considering the relative angle discrimination threshold of fingertip, an angle mapping strategy is employed to realize continuous multi-directional skin-slip. Two servo motors are equipped to drive the five-bar mechanism to provide normal indentation on the finger pulp. The characteristics of the device were obtained through the bench test. Three experiments were designed and conducted to evaluate the performance of the device. The results of the two-dimensional surface exploration (Exp #1) proved that the subjects could trace four paths and choose the appropriate score for the question. Besides, the device could effectively transmit continuous multi-directional skin-slip by collaborating with the angle mapping strategy. In the normal indentation experiment (Exp #2), the device was proved to be able to display the surfaces with different heights, and the subjects were able to distinguish the difference in height. In the three-dimensional surface exploration (Exp #3), the subjects did not have a reduced exploration efficiency on a specific contour. The overall average correct ratio for the contours was 73.3% (70% for the square, 60% for the circle, and 90% for the triangle). The current device proposed in this article can effectively transmit three-dimensional skin-slip display, but it has some limitations, such as unbalanced mass distribution and limited wearability. Future work will focus on the mechanism and actuation optimization to improve the wearability and compactness of the device.

REFERENCES

[1] A. Zenner, A. Makhsadov, S. Klingner, D. Liebemann, and A. Krüger, "Immersive process model exploration in virtual reality," *IEEE Trans. Vis. Comput. Graph.*, vol. 26, no. 5, pp. 2104–2114, May 2020.

[2] Y. Kamikawa and A. M. Okamura, "Comparison between force-controlled skin deformation feedback and hand-grounded kinesthetic force feedback for sensory substitution," *IEEE Robot. Automat. Lett.*, vol. 3, no. 3, pp. 2174–2181, Jul. 2018.

[3] J.-L. Rodríguez, R. Velázquez, C. Del-Valle-Soto, S. Gutiérrez, J. Varona, and J. Enríquez-Zarate, "Active and passive haptic perception of shape: Passive haptics can support navigation," *Electronics*, vol. 8, no. 3, 2019, Art. no. 355.

[4] A. B. Dhiab and C. Hudin, "Confinement of vibrotactile stimuli in narrow plates," in *Proc. IEEE World Haptics Conf.*, 2019, pp. 431–436.

[5] S. Handelzalts, G. Ballardini, C. Avraham, M. Pagano, M. Casadio, and I. Nisky, "Integrating tactile feedback technologies into home-based telerehabilitation: Opportunities and challenges in light of COVID-19 pandemic," *Front. Neurorobot.*, vol. 15, 2021, Art. no. 617636.

[6] C. Pacchierotti, S. Sinclair, M. Solazzi, A. Frisoli, V. Hayward, and D. Prattichizzo, "Wearable haptic systems for the fingertip and the hand: Taxonomy, review, and perspectives," *IEEE Trans. Haptics*, vol. 10, no. 4, pp. 580–600, Oct.–Dec. 2017.

[7] M. Salada, J. E. Colgate, P. Vishton, and E. Frankel, "An experiment on tracking surface features with the sensation of slip," in *Proc. IEEE 1st Joint Eurohaptics Conf. Symp. Haptic Devices Virtual Environ. Teleoperator Syst. World Haptics Conf.*, 2005, pp. 132–137.

[8] R. J. Webster III, T. E. Murphy, L. N. Verner, and A. M. Okamura, "A novel two-dimensional tactile slip display: Design, kinematics and perceptual experiments," *ACM Trans. Appl. Percep.*, vol. 2, no. 2, pp. 150–165, 2005.

[9] J.-Y. Lo, D.-Y. Huang, C.-K. Sun, C.-E. Hou, and B.-Y. Chen, "Rolling-stone: Using single slip taxel for enhancing active finger exploration with a virtual reality controller," in *Proc. 31st Annu. ACM Symp. User Interface Softw. Technol.*, 2018, pp. 839–851.

[10] E. Whitmire, H. Benko, C. Holz, E. Ofek, and M. Sinclair, "Haptic revolver: Touch, shear, texture, and shape rendering on a reconfigurable virtual reality controller," in *Proc. CHI Conf. Hum. Factors Comput. Syst.*, 2018, pp. 1–12.

[11] S. V. Salazar, C. Pacchierotti, X. de Tinguy, A. Maciel, and M. Marchal, "Altering the stiffness, friction, and shape perception of tangible objects in virtual reality using wearable haptics," *IEEE Trans. Haptics*, vol. 13, no. 1, pp. 167–174, Jan.–Mar. 2020.

[12] S. H. Atapattu, N. M. Senevirathna, H. L.U. Shan, T. B. T. Madusanka, T. D. Lalitharatne, and D. S. Chathuranga, "Design and development of a wearable haptic feedback device to recognize textured surfaces: Preliminary study," in *Proc. IEEE Int. Conf. Adv. Intell. Mechatron.*, 2017, pp. 16–21.

[13] O. Wells, T. Pipe, S. Dogramadzi, and M. Studley, "Sheartouch-towards a wearable tactile feedback device to provide continuous shear force sensation in real time," in *Proc. Annu. Conf. Towards Auton. Robotic Syst.* 2020, pp. 287–298.

[14] C. Ho, J. Kim, S. Patil, and K. Goldberg, "The slip-pad: A haptic display using interleaved belts to simulate lateral and rotational slip," in *Proc. IEEE World Haptics Conf.*, 2015, pp. 189–195.

[15] P. Zhang, M. Kamezaki, Y. Hattori, and S. Sugano, "A wearable fingertip cutaneous haptic device with continuous omnidirectional motion feedback," in *Proc. IEEE Int. Conf. Robot. Automat.*, 2022, pp. 8869–8875.

[16] F. Chinello, M. Malvezzi, C. Pacchierotti, and D. Prattichizzo, "A three DOFs wearable tactile display for exploration and manipulation of virtual objects," in *Proc. IEEE Haptics Symp.*, 2012, pp. 71–76.

[17] M. Solazzi, A. Frisoli, and M. Bergamasco, "Design of a cutaneous fingertip display for improving haptic exploration of virtual objects," in *Proc. IEEE 19th Int. Symp. Robot Hum. Interactive Commun.*, 2010, pp. 1–6.

[18] M. Gabardi, M. Solazzi, D. Leonardis, and A. Frisoli, "A new wearable fingertip haptic interface for the rendering of virtual shapes and surface features," in *Proc. IEEE Haptics Symp.*, 2016, pp. 140–146.

[19] Y. Tanaka, Y. Goto, and A. Sano, "Haptic display of micro surface undulation based on discrete mechanical stimuli to whole fingers," *Adv. Robot.*, vol. 31, no. 4, pp. 155–167, 2017.

[20] Y. Gaffary et al., "Toward haptic communication: Tactile alphabets based on fingertip skin stretch," *IEEE Trans. Haptics*, vol. 11, no. 4, pp. 636–645, Oct.–Dec. 2018.

[21] L. A. Jones and H. Z. Tan, "Application of psychophysical techniques to haptic research," *IEEE Trans. Haptics*, vol. 6, no. 3, pp. 268–284, Jul.–Sep. 2013.